nature nanotechnology

ARTICLES

PUBLISHED ONLINE: 28 SEPTEMBER 2015 | DOI: 10.1038/NNANO.2015.221

Nanoscale cation motion in TaO_x, HfO_x and TiO_x memristive systems

Anja Wedig[1†], Michael Luebben[1†], Deok-Yong Cho[2], Marco Moors[1], Katharina Skaja[1], Vikas Rana[1], Tsuyoshi Hasegawa[3], Kiran K. Adepalli[4,5], Bilge Yildiz[4,5], Rainer Waser[1,6] and Ilia Valov[1,6*]

A detailed understanding of the resistive switching mechanisms that operate in redox-based resistive random-access memories (ReRAM) is key to controlling these memristive devices and formulating appropriate design rules. Based on distinct fundamental switching mechanisms, two types of ReRAM have emerged: electrochemical metallization memories, in which the mobile species is thought to be metal cations, and valence change memories, in which the mobile species is thought to be oxygen anions (or positively charged oxygen vacancies). Here we show, using scanning tunnelling microscopy and supported by potentiodynamic current–voltage measurements, that in three typical valence change memory materials (TaO_x, HfO_x and TiO_x) the host metal cations are mobile in films of 2 nm thickness. The cations can form metallic filaments and participate in the resistive switching process, illustrating that there is a bridge between the electrochemical metallization mechanism and the valence change mechanism. Reset/Set operations are, we suggest, driven by oxidation (passivation) and reduction reactions. For the Ta/Ta_2O_5 system, a rutile-type TaO_2 film is believed to mediate switching, and we show that devices can be switched from a valence change mode to an electrochemical metallization mode by introducing an intermediate layer of amorphous carbon.

Redox-based ReRAM devices offer significant potential for use in future information technology as components for memory[1,2], logic[3,4] and neuromorphic[5–8] applications. The devices have a metal–(nano)electrolyte–metal arrangement, where the ion-transporting material often shows insulating properties on the macroscopic scale, but evolves into an ionic or mixed ionic–electronic conductor at nanoscale device dimensions. Mediated by ion transport processes in combination with internal redox reactions, resistance switching can be introduced in these devices (cells) due to the formation/dissolution of electron-conducting filaments, allowing for non-volatile information storage. The attractiveness of ReRAM devices lies in their low power consumption, subnanosecond switching times[9] and a conceptual scalability down to the atomic level[10].

Two fundamentally different types of switching mechanism have emerged depending on the part of the ReRAM cell predominantly involved in the redox process: the electrode metal (such as Cu or Ag) in the case of electrochemical metallization memories (ECMs) or the oxide layer serving as the (nano)electrolyte in the case of valence change memories (VCMs)[11]. Significant progress in understanding the kinetics of filament formation and the nature of the conductive filament on a microscopic level has been achieved for both types of ReRAM by applying highly resolved techniques such as local-conduction atomic force microscopy[12], transmission electron microscopy[13,14] and scanning tunnelling microscopy[15] (STM). However, reports on STM investigations of resistive switching are rare due to the low electronic conductivity of the solid electrolytes suppressing electron tunnelling. The studies are typically limited to materials with mixed conductivity (for example, Cu_2S (ref. 16) and Ag_2S (ref. 17)) or purely electronically conducting materials such as Nb-doped $SrTiO_3$ (ref. 18). A conceptual solution to overcome this problem for solid electrolytes was demonstrated for purely cation-conducting $RbAg_4I_5$ (ref. 15) and it has been suggested that a similar solution can be applied to VCM systems.

Typical VCM materials are transition metal and/or refractory oxides such as HfO_2, TiO_2 and Ta_2O_5 (ref. 19). The existence of cation defects in these types of oxide is well known, and the possibility of their involvement in VCM processes has not been excluded[11,20,21]. However, the formation of the filament, composed of a reduced (electronically conductive) metal oxide phase, and the switching phenomena in general are widely described to be related to redox reactions and the transport of oxygen ions or, in defect-chemical (Kroeger-Vink[22]) notation, oxygen vacancies as mobile donors. After formation, the filament should only be partially reoxidized, and a layer (disc) with a thickness of up to a few nanometres forms that is responsible for resistive switching. Thus, subsequent voltage manipulations—that is, Set and Reset operations—are supposed to be only due to the shift of oxygen vacancies under the applied electric field within this thin layer of partially reduced oxide[11].

STM switching and point contact formation

Figure 1 shows STM-tip-induced switching experiments on 2-nm-thin amorphous layers of TaO_x deposited on Ta bottom electrodes. The samples were vacuum-annealed to increase the conductivity in the oxide layer by partial reduction/forming. By preparing the samples in this way and with this thickness, we aimed to reproduce the conditions and properties of the metal oxide layer responsible for resistive switching in real devices. Cathodic or anodic bias voltages were applied to the STM tip at a fixed tip position and tip–sample distance to trigger the resistive switching event, and the time dependence of the resulting current was measured. The sample was initially exposed to an anodic tip voltage of 1 V (Fig. 1a,A), which

[1]Peter Gruenberg Institute, Research Centre Juelich, Juelich 52425, Germany. [2]Department of Physics, Chonbuk National University, Jeonju 561-756, Korea. [3]International Center for Materials Nanoarchitectonics, National Institute for Materials Science, 1-1 Namiki, Tsukuba, Ibaraki 305-0044, Japan. [4]Department of Nuclear Science and Engineering, 77 Massachusetts Avenue, Cambridge, Massachusetts 02139, USA. [5]Department of Materials Science and Engineering, Massachusetts Institute of Technology, 77 Massachusetts Avenue, Cambridge, Massachusetts 02139, USA. [6]Institute for Materials in Electrical Engineering II, RWTH Aachen University, Sommerfeldstrasse 24, Aachen 52074, Germany. †These authors contributed equally to this work. *e-mail: i.valov@fz-juelich.de

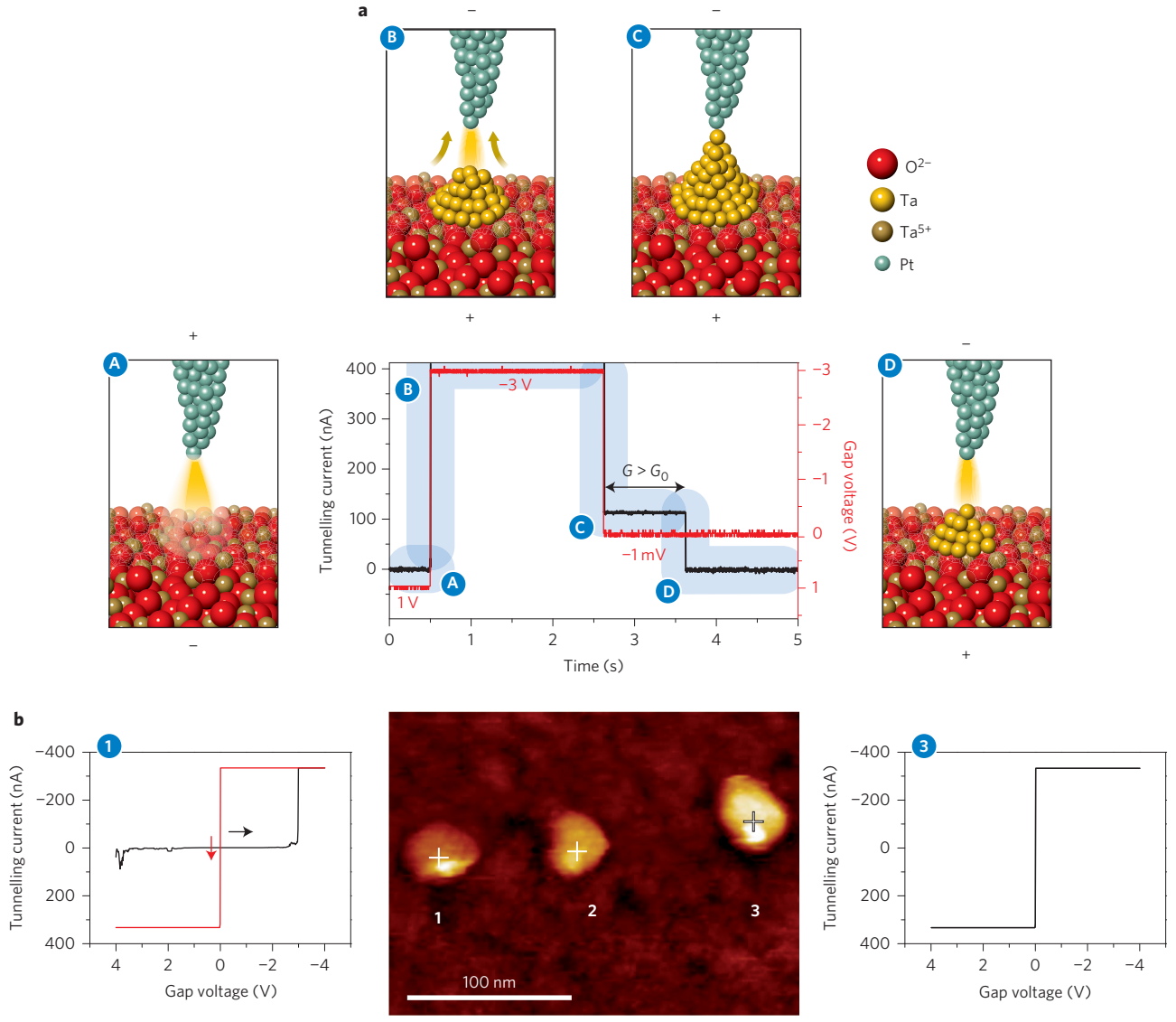

Figure 1 | Scanning tunnelling switching at negative tip voltages under UHV conditions. a, Time dependence of the tunnelling current measured on a 2-nm-thin TaO_x layer on changing the voltage applied to the STM tip stepwise from +1 V to −3 V to −1 mV. The conductance G calculated from the current at a tip voltage of −1 mV exceeds the conductance quantum G_0, indicating the formation of a metallic quantum point contact that is temporarily stable after removal of the high electric field. Contact formation is attributed to the diffusion of Ta ions to the negatively charged STM tip. **b**, Surface image of the TaO_x layer recorded directly after time-resolved STM measurements at negative tip voltages applying a scanning bias voltage of 1 V to the tip and with a tunnelling current setpoint of 1 nA. Highly conductive regions are visible at the positions where local resistive switching was performed. The size of the nuclei is comparable to those observed for other materials. The current–voltage curves measured on these regions show either purely metallic or mixed metallic–semiconducting behaviour, the latter suggesting a high tendency towards reoxidation of the metallic Ta structures formed during resistive switching.

proved to have no effect on the sample's morphology or electronic structure. On changing the tip voltage to −3 V, a strong increase in the current was detected (Fig. 1a,B), indicating resistive switching to the low-resistance state (LRS). A resistance of 9.6 kΩ (current of 104 nA at −1 mV) was measured after the pulse elapsed (Fig. 1a,C). This corresponds to a conductance higher than the atomic point contact quantum conductance G_0 ($G = 1.3G_0$).

This high conductance cannot be explained by the formation of an oxygen-deficient conductive filament in the oxide. It is instead a proof of the establishment of a metallic quantum point contact between the STM tip and the sample. By 'metallic contact', we mean the formation of a metallic Ta filament bridging the vacuum gap and providing direct galvanic contact to the tip via at least one Ta atom. The switching mechanism is comparable to that observed for gap-type atomic switches built from cation-conducting ECM cells[15,23]. The formation of an atomic point contact can only happen if two conditions are fulfilled simultaneously: (1) the metal cations are mobile within the TaO_x film and (2) the applied voltage is sufficient to increase the chemical potential of the electrons (Fermi level) to or above the energy level required for the reduction reaction $Ta^{5+} + 5e^- \rightarrow Ta$ to proceed. Consequently, the switching process in TaO_x under negative bias conditions has to be related to a movement of Ta ions to the STM tip and subsequent reduction, as encountered in gap-type ECM cells. Based on our experiments, we cannot determine for certain whether the cation defects are Ta vacancies or Ta interstitials. However, because of the small size of the Ta ions and the existence of a reduced, amorphous TaO_x phase (Ta interstitials are donors in the same way as the oxygen vacancies), we consider Ta interstitials to be the more probable cation defects. The metallic point contact remains stable for a certain period of time after removal of the electric field and then breaks (Fig. 1a,D). We explain this disruption of the metallic

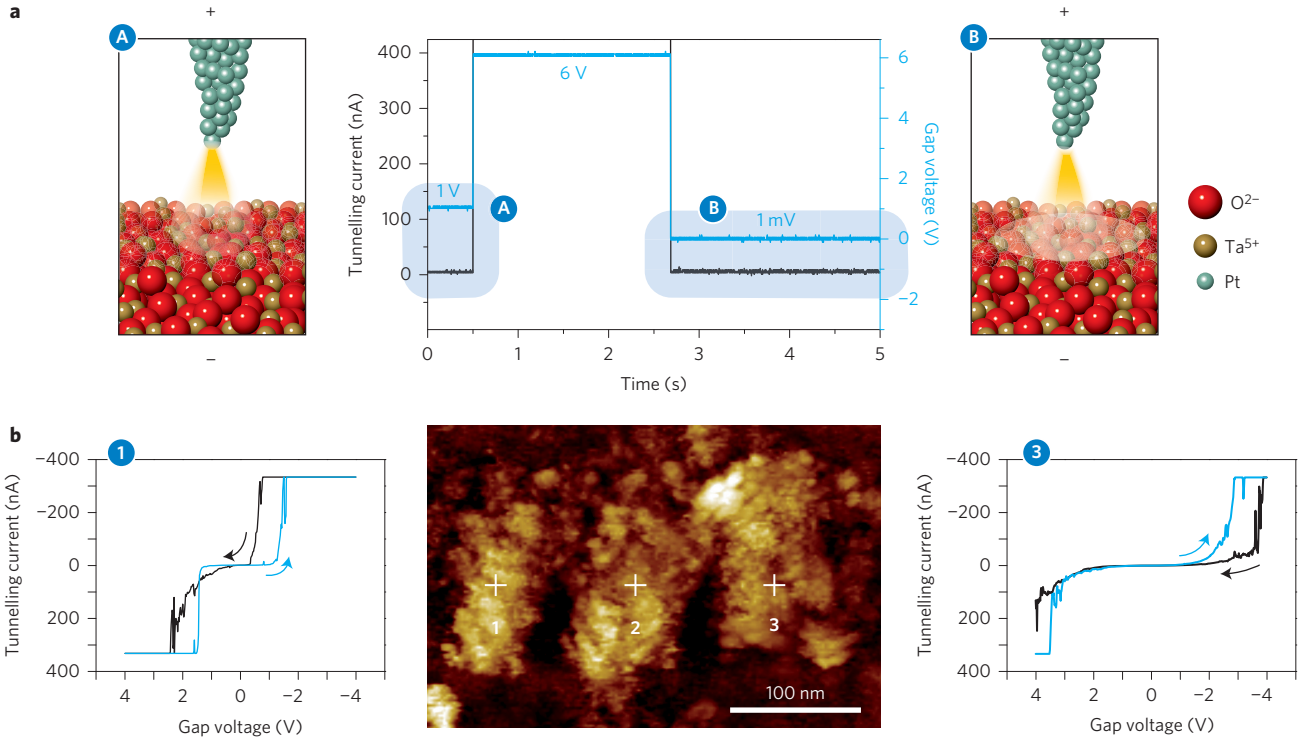

Figure 2 | Scanning tunnelling switching at positive tip voltages. a, *I*–*t* dependence measured on a TaO_x layer showing no quantum point contact after the voltage is decreased. The initial current increase is related to a different switching mechanism, possibly predominantly involving the diffusion of oxygen vacancies. **b**, Surface image of the TaO_x layer recorded directly after time-resolved STM measurements at positive tip voltages applying a scanning bias voltage of 1 V to the STM tip and with a tunnelling current setpoint of 1 nA. Diffuse conductive regions are visible at the positions where local resistive switching was performed. Current–voltage curves measured on these regions show semiconducting behaviour.

contact by the high tendency of the Ta nucleus to reoxidation even under ultrahigh-vacuum (UHV) conditions, as also suggested by the STM imaging.

Figure 1b presents a STM image of a 2-nm-thin TaO_x layer recorded after three consecutive local switching events at cathodic tip voltages. The switching leads to the formation of highly conductive regions with an average diameter of ~40 nm. The reproducibility of the features points to the applicability of this method in the rather young field of redox-based STM nanolithography[18,24]. Current–voltage spectroscopy performed on the modified areas in most cases revealed metallic conduction indicative of the local enrichment of Ta metal. At position 1 (switched first) we also observed semiconducting behaviour, but at position 3 (switched last) the behaviour is metallic. The semiconducting features at position 1 again suggest a high tendency of the metallic structures to reoxidation, in accordance with the limited stability of the metallic behaviour found in time-resolved measurements. The resistance at position 1 can again be changed into a metallic one by applying a cathodic voltage to the tip.

To exclude the effect of a possible asymmetric field gradient, we performed switching experiments by applying opposite (that is, positive) tip voltages of up to 6 V. We again observed a switching of the TaO_x layer to a LRS, indicated by the strong increase in the tunnelling current shown in Fig. 2a. However, the current was not sustained after the pulse elapsed (Fig. 2a,B) and thus no bridging of the tunnelling gap was observed. The STM image recorded after switching at 6 V at three different points again shows regions of increased conductivity (Fig. 2b), but the highly conducting areas are much broader than those in Fig. 1b, and *I*–*V* spectroscopy on the LRS regions showed predominantly semiconducting behaviour (for extended results see Supplementary Section 1). As the STM tip is positively polarized, the possible redox reaction at the tip is the oxidation of oxygen ions from TaO_x, whereas at the counterelectrode, the reduction of both residual oxygen and cations is possible. The much larger modified area depicts the field distribution at the large bottom electrode characterized by a much smaller current density. Thus, the switching of the sample at positive tip voltages has to be explained by a switching mechanism other than filament formation based on the redox reaction alone and the motion of host cations towards the metal electrode under the oxide layer.

Atomic point contacts on HfO_x and TiO_x films

The STM investigations performed on HfO_x and TiO_x layers yielded results comparable to those obtained for TaO_x. The application of a cathodic tip voltage resulted in the build-up of metallic quantum point contacts, which were stable for several seconds after removal of the electric field and were then disrupted (Fig. 3a,c). This indicates that for these materials also, the formation of a temporarily stable metallic filament via the diffusion of cations to the negatively charged STM tip is responsible for the observed resistance switching. As shown in Fig. 3b,d, the application of a positive voltage to the tip does not lead to the formation of metallic point contacts and the conductance values remain well below G_0, similar to the situation on TaO_x.

The STM studies on surface electrochemical processes are applicable to gapless-type systems, because fundamental properties of matter—that is, the mobility of ions, activation energies, rate constants and kinetic parameters for redox reactions for the studied systems—can be determined from the experimental data[15,25]. Thus, we provide clear evidence that the cations in thin films of TaO_x, HfO_x and TiO_x are mobile under the influence of an electric field and can actively participate in the resistive switching process in competition with the oxygen vacancies. We have also confirmed

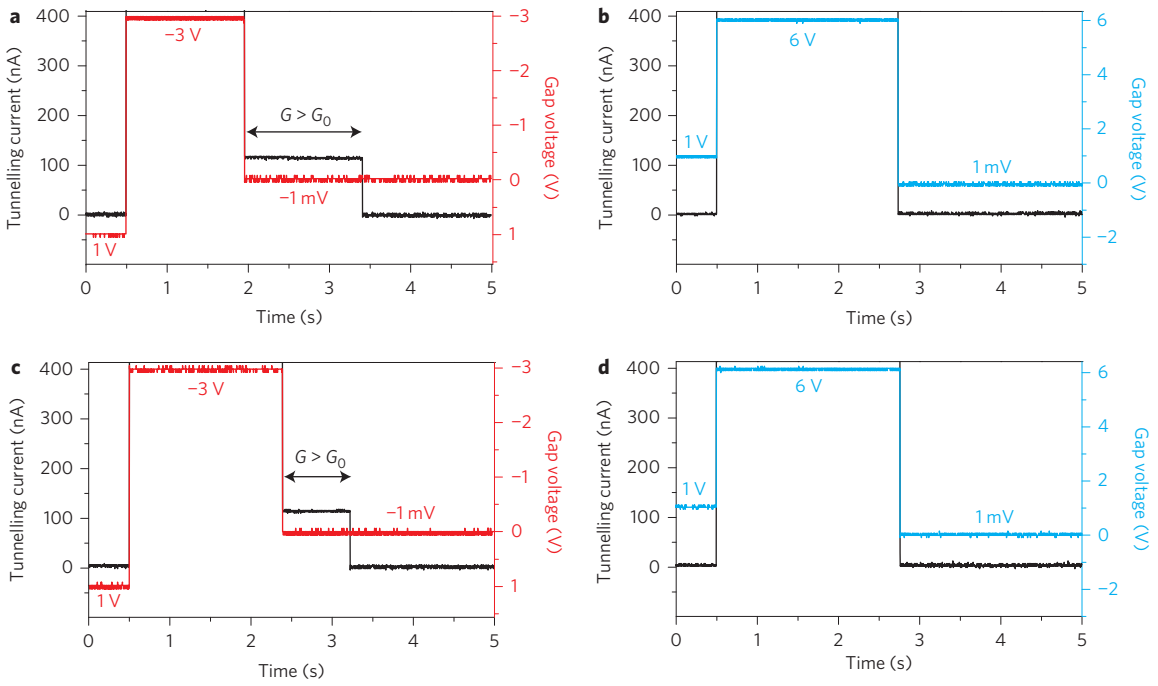

Figure 3 | Scanning tunnelling switching on HfO_x and TiO_x. a,b, Time dependence of the tunnelling current measured on a 2-nm-thin HfO_x layer on changing the voltage applied to the STM tip stepwise. **c,d**, Time dependence of the tunnelling current measured on a 2-nm-thin TiO_x layer. The behaviour of both metal oxides is qualitatively identical to that of TaO_x. The resistive switching at high negative tip voltages is attributed to the formation of a metal filament, also proving cation mobility for these materials. The polarity of the initial tip voltage does not have any (artificial) effect on the current–time characteristics.

that in 15 nm oxide thin films Ta ions are mobile, by carrying out diffusion experiments on NbO_x/TaO_x bilayer structures and secondary ion mass spectrometry (SIMS) depth profiling (for details see Supplementary Section 2).

Cation mobility in these oxides is also supported by studies on the passivation of metals (for example, Ta, Al and W) in liquid electrolytes, where cation diffusion coefficients (in dense oxide films) comparable to those of oxygen vacancies have been reported, obtained by tracer diffusion marker experiments[26–28]. A high cation mobility was furthermore observed for TiO_{2-x}, for example, in tracer diffusion experiments at high temperatures[29] (temperatures of up to 1,000 K can be induced in a VCM due to Joule heating), but also in thin films grown at room temperature[30–32]. Moreover, ECM-type behaviour and a metallic LRS at room temperature have recently been reported for VCM devices of the Ti/TiO_x system[33]. These results further support our findings, although the authors attributed them to an oxygen-vacancy-based mechanism.

Ta/Ta_2O_5 interface structure and switching

To relate the results obtained by STM to the behaviour of real devices (a larger electrode surface area with full electrode–electrolyte contact), we performed X-ray absorption studies focused on the structure of the Ta/Ta_2O_5 interface. We used X-ray absorption spectroscopy (XAS) as a non-destructive bulk-sensitive technique to examine the chemistry of the Ta/Ta_2O_5 system. As well as chemical analyses with X-ray absorption near-edge structure (XANES), we also obtained structural information from the extended X-ray absorption fine structures (EXAFS) presented in Fig. 4.

The Ta atoms at the Ta/Ta_2O_5 interface are much more disordered than those in the bulk Ta foil (Fig. 4a,b). This implies that a variety of local environments exist in the interfacial Ta layers. More detailed analyses have shown that the Ta layers near the Ta/Ta_2O_5 interface internally oxidize to form an intermediate rutile-type TaO_2 layer. As shown in Fig. 4c, the EXAFS analyses suggest that the TaO_2 layer has a short-range rutile structure, although the film is amorphous overall. XANES analyses have shown that this intermediate layer has a different electronic structure. Combined with the different short-range order, this different electronic structure is a prerequisite for different transport properties (more detailed XAS analyses are provided in Supplementary Section 3). The TaO_2 layer is formed spontaneously at the Ta/Ta_2O_5 interface and mediates the oxidation of Ta metal. TaO_2 is thermodynamically unstable, so structural studies on TaO_2 have rarely been reported, and no experimental results on ion or electron diffusion have been published. However, it easily oxidizes to insulating Ta_2O_5 in the presence of oxygen. As the oxidation of Ta is supported by the diffusion of both cations and anions, we believe that this intermediate layer is mainly responsible for the resistive switching (after the forming process) and allows the movement of both oxygen and tantalum ions, as well as electrons.

Figure 5 presents current–voltage curves and current–time transients of the Reset process measured on a $Ta/(TaO_2)Ta_2O_5/Pt$ cell. The cell consists of a 10 nm Ta_2O_5 layer deposited on platinized SiO_2 and covered with Ta electrodes (0.1–1 mm in diameter). Before the switching experiments, the cell was set into the LSR by applying a voltage of −5 V to the Pt electrode at a current compliance of 1 mA. Both plots in Fig. 5 show the behaviour to be expected for the passivation of a metal (which is well known from textbooks on liquid-phase electrochemistry) (Supplementary Section 4).

We performed Reset voltage sweeps to different positive voltage vertex values at the Pt electrode and observed a partial Reset of the cell to different high-resistance states (counter-eight-wise switching[34], Fig. 5a) corresponding to different stages of reoxidation of the filament. The particular resistance depends on the oxide layer thickness and/or composition, which in turn depends on the driving force for reoxidation (the applied voltage). We believe that the switching layer is mainly composed of the rutile-type TaO_2 phase. The LRS is then achieved either by the reduction of Ta ions to metallic Ta or the formation of Ta-ion-enriched TaO_2. The reoxidation (Reset) transforms it back into TaO_2/Ta_2O_5,

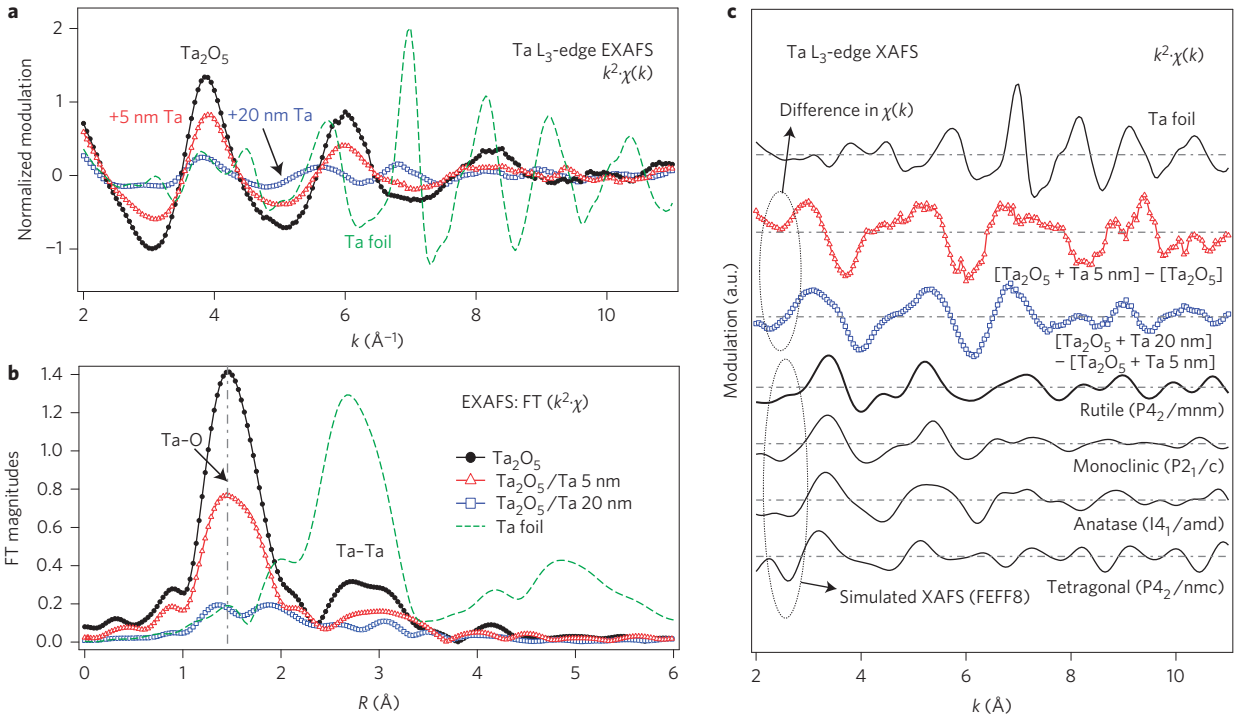

Figure 4 | EXAFS measurements at the Ta/Ta_2O_5 interface. a,**b**, Ta L_3-edge EXAFS modulations $\chi(k)$, normalized by edge jumps and weighted by k^2 (**a**) and their Fourier-transformed (FT) modulations of the Ta_2O_5 films before and after 5 or 20 nm Ta deposition (**b**). The spectra of Ta foil are included for comparison. The overall features, except the first-shell features (Ta–O), are much weaker than those of the Ta foil, suggesting that all films had a high degree of structural disorder due to amorphousness. It is clear that the first-shell feature of the Ta_2O_5 + (5 nm Ta) sample is much weaker (approximately half) and that of the Ta_2O_5 + (20 nm Ta) sample is even weaker (approximately one-tenth) than that of the Ta_2O_5 sample. This is the consequence of an increasing fraction of Ta metal with respect to the Ta oxide as the Ta thickness increases. Furthermore, the weak second-shell feature (Ta–Ta) even in the Ta_2O_5 + (20 nm Ta) sample implies that the deposited Ta metal layers are much more disordered than those in the bulk Ta foil. **c**, Difference XAFS of the Ta_2O_5 + (Ta 5 nm) and Ta_2O_5 + (Ta 20 nm) films received by subtracting the XAFS modulations of the Ta_2O_5 and Ta_2O_5 + (Ta 5 nm) films, respectively. The XAFS modulation of the Ta foil is provided for comparison. Results of theoretical simulations (FEFF8) for possible TaO_2 phases with various crystal structures are also shown. The XAFS modulation of the rutile structure is similar to that of the experimental difference XAFS, suggesting the prevalence of a rutile-type TaO_2 phase at the Ta_2O_5/Ta interface.

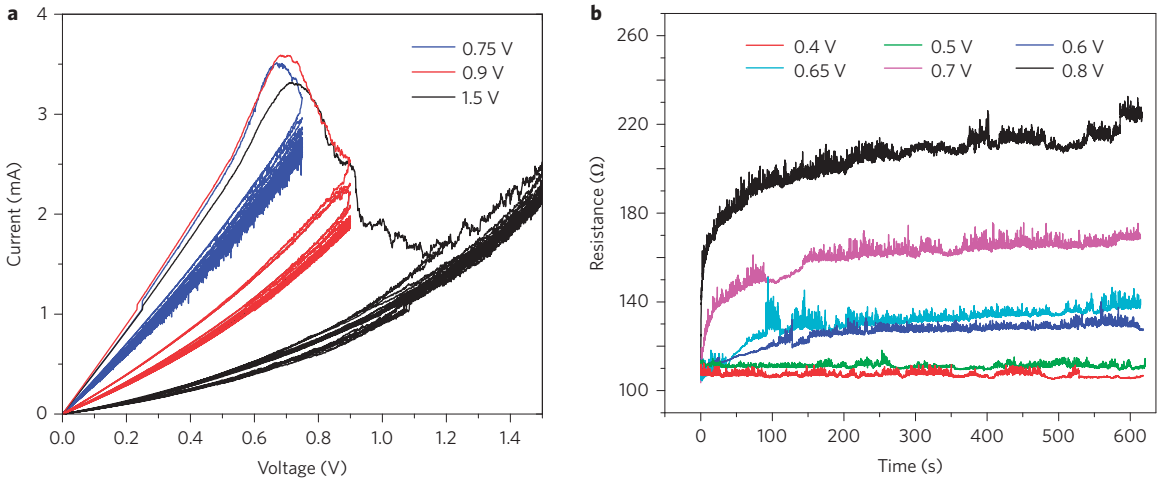

Figure 5 | Reset behaviour of TaO_x-based devices. a, Reset curves obtained on sweeping to different positive maximum voltages. The cell was formed at a negative voltage and Set to a LRS before each sweep series with different maximum voltage. In the first cycle of each sweep series, an increase in the slope appears before the maximum current is reached. The effect is attributed to the passivation of the conductive filament. **b**, Time dependence of the resistance at different applied constant voltages. At high voltage values, the resistance increases with time due to the formation of the passive layer. Voltage values refer to the Pt electrode.

increasing the total cell resistance. The achieved intermediate states proved to be stable following repeated cycles to the respective maximum voltage, without self-switching of the cell to different LRS. These states can also be reproducibly generated on the same cell if, after the Set, we Reset the cell and apply the same conditions. In this way, we can precisely control the resistance of the off state.

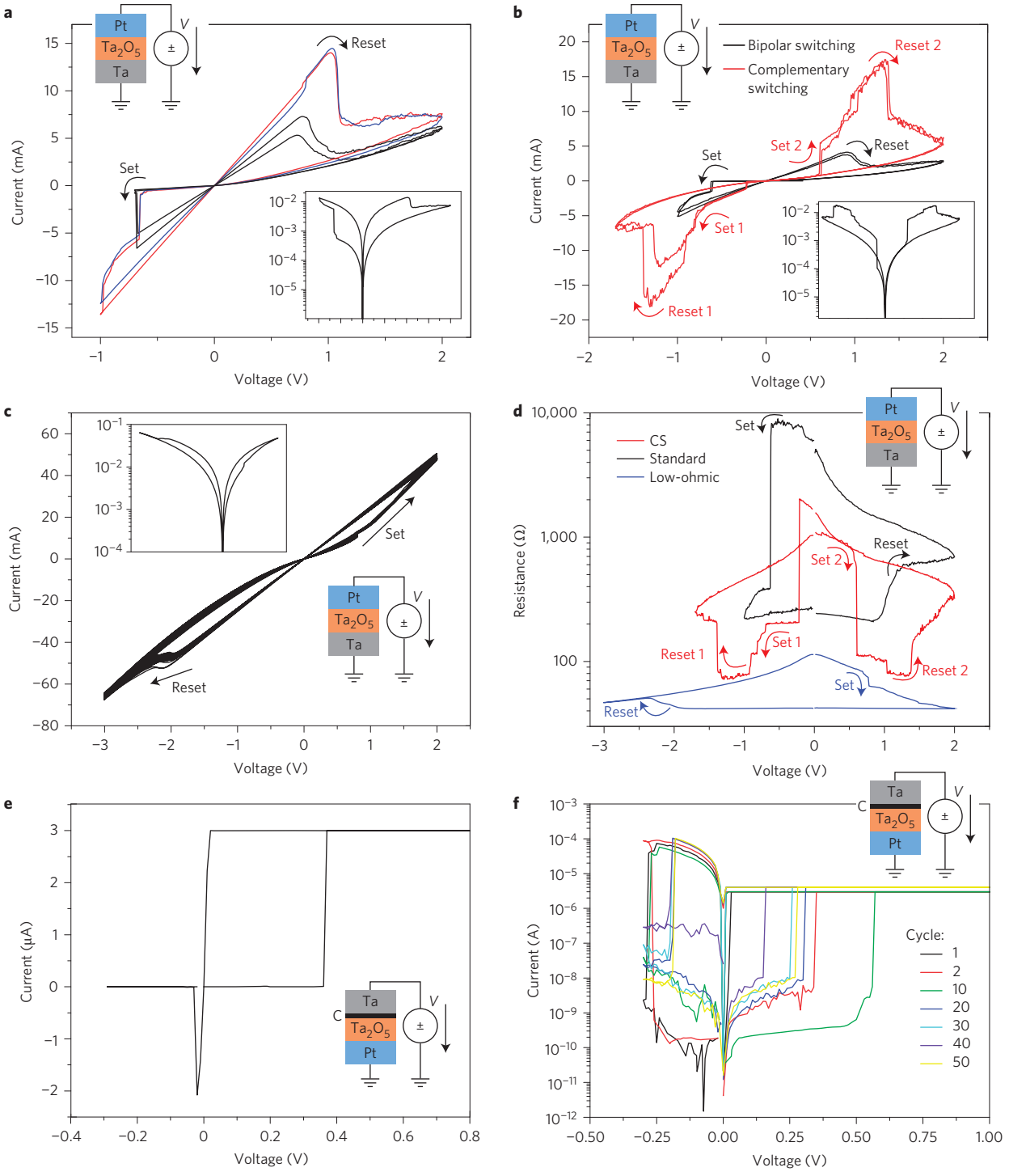

Figure 6 | *I–V* sweeps on TaO_x-based devices. a, Typical bipolar switching curves obtained on sweeping to low maximum voltages in the Set direction. Before the switching experiments, the cell was formed into a LRS applying a voltage of –5 V at a current compliance of 1 mA. During sweeping, a gradual transfer to two different LRSs is observed. A logarithmic depiction of a bipolar switching curve is shown in the inset. **b**, Complementary switching curves recorded on sweeping to a moderate negative maximum voltage. Bipolar switching curves measured on the same cell are shown for comparison. **c**, Highly conducting bipolar switching curves with reversed switching polarity obtained on sweeping to a high negative maximum voltage at low sweep rates. A low sweep rate is necessary to avoid a hard breakdown of the cell coinciding with morphological changes. **d**, Comparison of resistances calculated from the different types of switching curve. The low resistance values associated with the highly conducting switching behaviour and the two LRSs of the complementary switching cells indicate metallic-type electrical conduction via a filament. **e**, ECM-type switching demonstrated on a Ta/C/Ta_2O_5/Pt cell. **f**, Cycling a Ta/C/Ta_2O_5/Pt cell in ECM mode for 50 cycles shows a resistance window of up to 10^6 Ω.

The same passivation-type behaviour is observed in the *I–t* relaxation curves at constant applied positive voltage shown in Fig. 5b. A higher applied voltage resulted in a lower relaxation current, corresponding to a higher resistance and a higher degree of reoxidation and/or film thickness. The observation of a passivation-type behaviour shows that in the TaO_x device, the switching cannot

only be due to a simple shift of ionic defects, but involves a redox reaction and the formation and reoxidation of metallic Ta or reduced TaO_x phases. Similar passivation-type I–V curves were also recorded for Ta/Ta_2O_5 cells measured with different current compliances as well as Hf/HfO_x- and Ti/TiO_x-based VCM devices (Supplementary Section 5).

To examine the type of conductivity of the filament, we performed temperature-dependent (180–373 K) measurements of the LRS (Supplementary Section 6), showing metallic behaviour at temperatures below 298 K. In the temperature range 298–373 K, the LRS was not stable for more than ~15 min and the data scatter. The strongly negative Gibbs energy of formation for Ta_2O_5, $\Delta_f G = -760$ kJ mol^{-1} (corresponding to an oxygen activity of 10^{-133}), indicates that the metallic Ta filament tends to oxidize, as also observed in STM and XAS measurements. The same behaviour is expected and observed for Hf/HfO_x and Ti/TiO_x systems with Gibbs energies of formation of $\Delta_f G = -1{,}010$ kJ mol^{-1} and $\Delta_f G = -888$ kJ mol^{-1}, respectively (Supplementary Section 7). Therefore, we cannot provide an unequivocal answer as to whether the (electronically conducting) filament in real devices (if formed metallic) remains metallic or partially oxidizes.

Competition/transition between VCM and ECM switching

The potentiodynamic experiments (I–V sweeps) presented in Fig. 6 revealed new features confirming that different mechanisms of resistive switching are present, which are related to the contributions of the two mobile ionic species, that is, oxygen and tantalum ions.

Figure 6a presents bipolar switching curves measured on a negatively formed Ta/(TaO_2)Ta_2O_5/Pt cell. The I–V sweep experiments typically shown in the literature were extended by increasing the sweep range during consecutive sweep cycles. The expected cell performance was verified during the first voltage sweeps, where the cell was Reset to a high-resistance state (HRS) at positive voltages, and the negative sweeps Set the cell back to the LRS (counter-eightwise switching) with a resistance of ~120 Ω calculated from the slope of the I–V curves in the ohmic regime. In subsequent cycles, the voltage range in the Set direction was increased, resulting in states with a lower resistance down to ~80 Ω indicated by the steeper slope of the I–V curves. Accordingly, the Reset voltages were shifted to higher positive values. This behaviour (as well as Fig. 5) also demonstrates the facility of the cell for multi-level switching operations.

Completely different switching characteristics were found when the maximum sweep voltage in the Set direction was increased further. On sweeping to a moderate maximum voltage (in this particular case to −1.6 V), we observed a complementary switching behaviour[35], where the cell is Set at a lower voltage and Reset at a higher voltage of the same polarity (Fig. 6b). The low resistance values associated with the two LRSs of ~100 Ω (Fig. 6d) are again an indication of metallic-type electrical conduction via a filament. As the two Set events occur at different absolute voltage values, a thermochemical switching mechanism can be excluded. The two Reset events, on the other hand, occur at the same voltage values, indicating a thermally assisted mechanism. The complementary switching behaviour can be well explained either by the movement of oxygen vacancies only or cation defects only, or by the movement of both charged species. However, the versatile switching behaviour demonstrated for the TaO_x cells, as well as its complexity, can be explained reasonably by only taking into account that both cations and anions are involved in the resistive switching.

When voltage sweeps were performed to even higher negative voltage values at a sufficiently low sweep rate (0.25 V s^{-1}), bipolar switching with highly conducting LRS/HRS was observed (Fig. 6c), showing a smaller hysteresis and a reversed switching polarity with respect to the bipolar case described above (eightwise switching[34,36]). The low resistance values in the range of 40–100 Ω point to a metallic conduction pathway, as also reported for TiO_2-based cells[33].

We also succeeded in inducing and demonstrating the ECM mode in the devices by introducing a thin intermediate layer of amorphous carbon between the Ta and Ta_2O_5. The I–V sweeps in Fig. 6e,f show typical ECM characteristics with asymmetric Set/Reset voltages and currents. The Reset currents vary, ranging from I_{reset} comparable to the current compliance (Fig. 6e) to a much higher I_{reset} (Fig. 6f). This variability affects the Reset kinetics and ion transport due to the influence of Joule heating (for currents higher than ~10 μA) and the higher partial electronic current (which in turn increases the Reset voltage). Indeed, for small I_{reset} (Fig. 6e), V_{reset} is nearly 10 times lower than V_{reset} for higher I_{reset}. The reason for this variability is statistical deviation from cell to cell, but it is important to note that the Set/Reset currents depend strongly on the material system. Thus, in ECM cells based on a TaO_x electrolyte, higher Reset currents are more typical, but lower values of I_{reset} have also been reported, for example, in Cu/TaO_x/Pt ECM cells[37–39]. The Ta/C/TaO_x/Pt system (assuming mobile Ta ions) shows I–V characteristics almost identical to those reported for the Cu/TaO_x/Pt cells (assuming mobile Cu ions).

The Form voltages are the same as in the other devices, that is, $V_{form} = 5$ V (at the Ta electrode), but the Set voltages are much lower, varying between $V_{set} = 0.2$ V and 0.4 V at current compliances in the range 1–10 μA. The on/off resistance ratio can be as high as $R_{off}/R_{on} = 10^6$ (Fig. 6f). We tested the cells for up to 100 cycles and observed good stability, but deviation of V_{set}. We proved that the ECM mode works only if the amorphous carbon is positioned at the Ta/Ta_2O_5 interface (Ta/C/Ta_2O_5/Pt). Stacks of the type C/Ta/Ta_2O_5/C or Pt/C/Ta_2O_5/Pt do not provide ECM-mode switching.

We introduced the carbon layer to prevent a chemical reaction between the oxygen and tantalum (passivation) on applying Form and Set voltages (positive) to the Ta electrode. In ECM cells (using Ag or Cu active electrodes), during Set/Reset operations with counterelectrodes of metals with high oxygen affinity (for example, Ta, Al), we have previously found that the cell passivates on cycling[40]. As the equilibrium potential of the Ta^{5+}/Ta (as well as Hf^{4+}/Hf and Ti^{4+}/Ti) half-cell reaction is much more negative than that of the half-cell reaction O_2/O^{2-}, the first reaction on applying a positive voltage to the top electrode will be $Ta - 5e^- \rightarrow Ta^{5+}$. Afterwards, if oxygen ions are available, TaO_x will form (chemical step). At much higher potentials, oxygen ions can be oxidized: $2O^{2-} - 4e^- \rightarrow O_2$. Thus, our idea is to modify (decrease) the interface dynamics at the Ta/Ta_2O_5 interface and to suppress the oxygen reaction (for a detailed discussion see Supplementary Section 8). We have applied a similar concept to the system Ag/GeS_x, where we introduced a metallic layer at the Ag/GeS_x interface to stop the chemical reaction between Ag and GeS_x[41]. In this system we observed a stabilization of the on state, and suggested that the main role for this stabilization is a retarded diffusion of the metal component through the barrier layer. We therefore applied the same concept to VCM systems, and this has allowed us to demonstrate the transition to an ECM switching mode in the Ta_2O_5 system.

Conclusions

In view of the results of the nanoscale and macroscopic measurements, we conclude that the resistive switching in TaO_x, HfO_x and TiO_x can be caused not only by the diffusion of oxygen vacancies (as thought previously), but also by the migration of cations. Both processes lead to the formation of a highly reduced filament, creating a pathway for fast electrical conduction. A complete transition from a VCM switching mode to an ECM switching mode is demonstrated for a Ta/Ta_2O_5 device by introducing an intermediate layer of amorphous carbon, tuning the interface dynamics. The current–voltage characteristics may thus show features of ECM- and VCM-type

memristive switching depending on the boundary conditions. We relate one of the reasons for the high cation mobility in the Ta/Ta_2O_5 system to the intermediate TaO_2 layer, with rutile-type short-range order allowing both ions to move.

Filaments formed at negative STM tip voltages are metallic, but easily reoxidize, whereas LRS formed at positive tip voltages show different band structures with semiconducting, but also metallic-like behaviour. We conclude that the filament in the relaxed state is chemically inhomogeneous and composed of regions at different stages of oxidation. The participation of both cations and anions in the switching process in oxide-based cells can also explain the complexity of the observed switching phenomena. Additionally, the observation of field-induced morphological changes is important for redox-based STM nanolithography on metal oxides. The results we report provide fundamentally new insight into the resistive switching mechanism in oxide-based ReRAMs and should be used for improved device design and modelling.

Methods

Methods and any associated references are available in the online version of the paper.

Received 3 October 2014; accepted 25 August 2015; published online 28 September 2015

References

1. Baek, I. G. *et al.* Highly scalable non-volatile resistive memory using simple binary oxide driven by asymmetric unipolar voltage pulses. *IEDM Tech. Dig.* 587–590 (2004).
2. Waser, R. & Aono, M. Nanoionics-based resistive switching memories. *Nature Mater.* **6,** 833–840 (2007).
3. Kaeriyama, S. *et al.* A nonvolatile programmable solid–electrolyte nanometer switch. *IEEE J. Solid-State Circ.* **40,** 168–176 (2005).
4. Strukov, D. B. & Likharev, K. K. CMOL FPGA: a reconfigurable architecture for hybrid digital circuits with two-terminal nanodevices. *Nanotechnology* **16,** 888–900 (2005).
5. Foelling, S., Tuerel, O. & Likharev, K. Single-electron latching switches as nanoscale synapses. *Proc. IJCNN'01*, 216–221 (2001).
6. Pickett, M. D., Medeiros-Ribeiro, G. & Williams, R. S. A scalable neuristor built with Mott memristors. *Nature Mater.* **12,** 114–117 (2013).
7. Jo, S. H. *et al.* Nanoscale memristor device as synapse in neuromorphic systems. *Nano Lett.* **10,** 1297–1301 (2010).
8. Ohno, T. *et al.* Short-term plasticity and long-term potentiation mimicked in single inorganic synapses. *Nature Mater.* **10,** 591–595 (2011).
9. Torrezan, A. C., Strachan, J. P., Medeiros-Ribeiro, G. & Williams, R. S. Sub-nanosecond switching of a tantalum oxide memristor. *Nanotechnology* **22,** 485203 (2011).
10. Hasegawa, T., Terabe, K., Tsuruoka, T. & Aono, M. Atomic switch: atom/ion movement controlled devices for beyond von-Neumann computers. *Adv. Mater.* **24,** 252–267 (2012).
11. Waser, R., Bruchhaus, R. & Menzel, S. in *Nanoelectronics and Information Technology* (ed. Waser, R.) 683–710 (Wiley, 2012).
12. Szot, K., Speier, W., Bihlmayer, G. & Waser, R. Switching the electrical resistance of individual dislocations in single-crystalline $SrTiO_3$. *Nature Mater.* **5,** 312–320 (2006).
13. Yang, Y. *et al.* Electrochemical dynamics of nanoscale metallic inclusions in dielectrics. *Nature Commun.* **5,** 4232 (2014).
14. Park, G.-S. *et al. In situ* observation of filamentary conducting channels in an asymmetric Ta_2O_{5-x}/TaO_{2-x} bilayer structure. *Nature Commun.* **4,** 2382 (2013).
15. Valov, I. *et al.* Atomically controlled electrochemical nucleation at superionic solid electrolyte surfaces. *Nature Mater.* **11,** 530–535 (2012).
16. Nayak, A., Tsuruoka, T., Terabe, K., Hasegawa, T. & Aono, M. Switching kinetics of a Cu_2S-based gap-type atomic switch. *Nanotechnology* **22,** 235201 (2011).
17. Nayak, A. *et al.* Rate-limiting processes determining the switching time in a Ag_2S atomic switch. *J. Phys. Chem. Lett.* **1,** 604–608 (2010).
18. Chen, Y. L. *et al.* Scanning tunneling microscopy/spectroscopy studies of resistive switching in Nb-doped $SrTiO_3$. *J. Appl. Phys.* **112,** 023703 (2012).
19. Yang, J. J., Strukov, D. B. & Stewart, D. R. Memristive devices for computing. *Nature Nanotech.* **8,** 13–24 (2013).
20. Yang, J. J. *et al.* High switching endurance in TaO_x memristive devices. *Appl. Phys. Lett.* **97,** 232102 (2010).
21. Balatti, S., Larentis, S., Gilmer, D. C. & Ielmini, D. Multiple memory states in resistive switching devices through controlled size and orientation of the conductive filament. *Adv. Mater.* **25,** 1474–1478 (2013).
22. Kroeger, F. A. *The Chemistry of Imperfect Crystals* (North-Holland, 1973).
23. Terabe, K., Hasegawa, T., Nakayama, T. & Aono, M. Quantized conductance atomic switch. *Nature* **433,** 47–50 (2005).
24. Chien, T., Santos, T. S., Bode, M., Guisinger, N. P. & Freeland, J. W. Controllable local modification of fractured Nb-doped $SrTiO_3$ surfaces. *Appl. Phys. Lett.* **95,** 163107 (2009).
25. Valov, I. *et al.* Atomic scale and interface interactions in redox-based resistive switching memories. *ECS Trans.* **64,** 3–18 (2014).
26. Davies, J. A., Domeij, B., Pringle, J. P. S. & Brown, F. The migration of metal and oxygen during anodic film formation. *J. Electrochem. Soc.* **112,** 675–680 (1965).
27. Verkerk, B., Winkel, P. & de Groot, D. G. On the mechanism of anodic oxidation of tantalum. *Phillips Res. Rep.* **13,** 506–508 (1958).
28. Whitton, J. L. The measurement of ionic mobilities in the anodic oxides of tantalum and zirconium by a precision sectioning technique. *J. Electrochem. Soc.* **115,** 58–61 (1968).
29. Venkatu, D. A. & Poteat, L. E. Diffusion of titanium in single crystal rutile. *Mater. Sci. Eng.* **5,** 258–262 (1970).
30. Khalil, N. & Leach, J. The anodic-oxidation of valve metals 1. Determination of ionic transport numbers by alpha-spectrometry. *Electrochim. Acta* **31,** 1279–1285 (1986).
31. Habazaki, H. *et al.* Ionic transport in amorphous anodic titania stabilised by incorporation of silicon species. *Corrosion Sci.* **44,** 1047–1055 (2002).
32. Akse, J. R. & Whitehurst, H. B. Diffusion of titanium in slightly reduced rutile. *J. Phys. Chem. Solids* **39,** 457–465 (1978).
33. Hu, C. *et al.* Highly controllable and stable quantized conductance and resistive switching mechanism in single-crystal TiO_2 resistive memory on silicon. *Nano Lett.* **14,** 4360–4367 (2014).
34. Shibuya, K., Dittmann, R., Mi, S. & Waser, R. Impact of defect distribution on resistive switching characteristics of Sr_2TiO_4 thin films. *Adv. Mater.* **22,** 411–414 (2010).
35. Linn, E., Rosezin, R., Kügeler, C. & Waser, R. Complementary resistive switches for passive nanocrossbar memories. *Nature Mater.* **9,** 403–406 (2010).
36. Muenstermann, R., Menke, T., Dittmann, R. & Waser, R. Coexistence of filamentary and homogeneous resistive switching in Fe-doped $SrTiO_3$ thin-film memristive devices. *Adv. Mater.* **22,** 4819–4822 (2010).
37. Tsuruoka, T. *et al.* Effects of moisture on the switching characteristics of oxide-based, gapless-type atomic switches. *Adv. Funct. Mater.* **22,** 70–77 (2012).
38. Tsuruoka, T., Terabe, K., Hasegawa, T. & Aono, M. Temperature effects on the switching kinetics of a Cu-Ta_2O_5-based atomic switch. *Nanotechnology* **22,** 254013 (2011).
39. Tsuruoka, T., Terabe, K., Hasegawa, T. & Aono, M. Forming and switching mechanisms of a cation-migration-based oxide resistive memory. *Nanotechnology* **21,** 425205 (2010).
40. Tappertzhofen, S., Waser, R. & Valov, I. Impact of counter electrode material on the redox processes in resistive switching memories. *ChemElectroChem* **1,** 1287–1292 (2014).
41. Van den Hurk, J. *et al.* Physical origins and suppression of Ag dissolution in GeS_x-based ECM cells. *Phys. Chem. Chem. Phys.* **16,** 18217–18225 (2014).

Acknowledgements

This study was financially supported in part by BMBF project no. 03X0140 and DFG priority programme SFB 917. B.Y. and K.K.A. also acknowledge financial support from the MIT MRSEC through the MRSEC Program of the National Science Foundation under award no. DMR-1419807.

Author contributions

I.V. conceived the idea and designed the study. A.W. and M.M. performed the STM experiments. M.L. conducted current–voltage measurements on TaO_x devices. D.-Y.C. performed and interpreted the XAS measurements. K.S. prepared the samples for the STM experiments. V.R. performed *I–V* sweeps on TaO_x, HfO_x and TiO_x devices. T.H., K.K.A. and B.Y. contributed to interpretation of the STM results. A.W. and I.V. wrote the manuscript. R.W. and I.V. directed the research. All authors contributed to the discussion of the results and improved the text.

Additional information

Supplementary information is available in the online version of the paper. Reprints and permissions information is available online at www.nature.com/reprints. Correspondence and requests for materials should be addressed to I.V.

Competing financial interests

The authors declare no competing financial interests.

Methods

Sample preparation for STM measurements. A 100-nm-thin Pt layer (providing electrical contact to the sample bottom) with dimensions of 1×0.2 cm^2 was deposited by sputter deposition onto a Si substrate with dimensions of 1×1 cm^2 covered by a 430-nm-thin layer of thermally grown SiO_2. The Pt contact layer was covered one-third with standard photoresist for a later liftoff procedure. Then, a 50-nm-thin layer of Ta, Hf or Ti was deposited by d.c. sputtering in Ar at a gas pressure of 7×10^{-3} mbar. A ~2-nm-thin layer of TaO_x, HfO_x or TiO_x was then deposited *in situ* by reactive d.c. sputtering in an atmosphere containing 75% Ar and 25% O_2 at a pressure of 3.5×10^{-2} mbar. The deposition duration for the oxide layer was extrapolated from the deposition duration for slightly thicker films (10–15 nm) determined via X-ray reflectometry and TEM of thin-film cross-sections. Finally, the Pt contact layer was accessed by a liftoff process in acetone and isopropanol.

Sample preparation for *I–V* sweeps. As a counter electrode, a 30-nm-thin Pt layer (r.m.s. surface roughness <1 nm) was desposited by sputter deposition onto a Si substrate with dimensions of 1×1 in^2 covered by 430 nm thermally grown SiO_2 and a 5-nm-thin adhesion layer of TiO_2. Thereafter, a 10 nm TaO_x layer was deposited by reactive radiofrequency (RF) sputtering. Subsequently, 15-nm-thin Ta top electrodes with a diameter of 0.1–1 mm encapsulated by 30 nm Pt were prepared using conventional ultraviolet lithography and RF sputtering in Ar at a pressure of 4×10^{-3} mbar, followed by a liftoff in acetone and isopropanol.

STM measurements. The STM experiments were carried out at room temperature in an Omicron VT scanning probe microscope operated at a base pressure of 5×10^{-10} mbar. A Tektronix TPS 2024 digital oscilloscope was used for the simultaneous recording of the tunnelling current and gap voltage during the time-resolved measurements. To clean the *ex situ* prepared oxide layers of surface adsorbates and to slightly increase the electrical conductivity, the samples were annealed at 550 °C for 1 h in ultrahigh vacuum before STM measurements. The switching experiments with a mechanically cut Pt/Ir tip as the top electrode were then performed according to the following procedure. After establishing stable tunnelling conditions at a fixed tip position applying a bias voltage of 1 V (referenced to the STM tip) and a tunnelling current setpoint of 1 nA, the feedback loop was switched off to fix the tip–sample distance. By stepwise changing the tip voltage from −6 V to +6 V, the switching event was initiated, as indicated by an increase in the measured current to the detection limit of the preamplifier (~450 nA). To calculate the local resistance of the sample in the switched area, the absolute current values were detected at a lower voltage in the millivolt regime.

***I–V* sweeps.** *I–V* sweeps were performed using a Keithley 6430 Subfemto Sourcemeter. In an initial electroforming step, the samples were switched to a LRS applying a voltage of −5 V to the Pt electrode with a current compliance of 1 mA. No current compliance was used in the subsequent current–voltage measurements.

X-ray absorption spectroscopy. Ta L_3-edge XAS was performed at the 10C beamline of the Pohang Light Source. The total fluorescence yields were collected using a Si detector. To enhance the sensitivity of the signals near the surface, a grazing-incidence X-ray geometry was used with an incidence angle of 3°. Depth-resolved information was obtained from the metal/oxide interface by varying the thickness of the metal (5–20 nm) and oxide (10–30 nm) layers. The samples were prepared in the same way as for the electrical measurements.